Biochimica et Biophysica Acta 1818 (2012) 2290–2301

Contents lists available at SciVerse ScienceDirect

Biochimica et Biophysica Acta

journal homepage: www.elsevier.com/locate/bbamem

Mapping of unfolding states of integral helical membrane proteins by GPS-NMR and scattering techniques: TFE-induced unfolding of KcsA in DDM surfactant

Antonello Calcutta [a], Christian M. Jessen [b], Manja Annette Behrens [b], Cristiano L.P. Oliveira [b,1], Maria Lourdes Renart [c], José M. González-Ros [c], Daniel E. Otzen [d], Jan Skov Pedersen [b], Anders Malmendal [a,e,*], Niels Chr. Nielsen [a,*]

[a] Center for Insoluble Protein Structures (inSPIN), Interdisciplinary Nanoscience Center (iNANO) and Department of Chemistry, Aarhus University, Denmark
[b] Department of Chemistry and Interdisciplinary Nanoscience Center (iNANO), Aarhus University, Denmark
[c] Instituto de Biología Molecular y Celular, Universidad Miguel Hernández, Elche (Alicante), Spain
[d] Center for Insoluble Protein Structures (inSPIN), Interdisciplinary Nanoscience Center (iNANO) and Department of Molecular Biology, Aarhus University, Denmark
[e] Department of Biomedical Sciences, Faculty of Health Sciences, University of Copenhagen, DK-2200 Copenhagen N, Denmark

ARTICLE INFO

Article history:
Received 16 January 2012
Received in revised form 23 March 2012
Accepted 9 April 2012
Available online 14 April 2012

Keywords:
KcsA–surfactant complex
TFE-induced unfolding
PCA
DDM micelle
Dynamic light scattering
Small-angle X-ray scattering

ABSTRACT

Membrane proteins are vital for biological function, and their action is governed by structural properties critically depending on their interactions with the membranes. This has motivated considerable interest in studies of membrane protein folding and unfolding. Here the structural changes induced by unfolding of an integral membrane protein, namely TFE-induced unfolding of KcsA solubilized by the n-dodecyl β-D-maltoside (DDM) surfactant is investigated by the recently introduced GPS-NMR (Global Protein folding State mapping by multivariate NMR) (Malmendal et al., PlosONE 5, e10262 (2010)) along with dynamic light scattering (DLS) and small-angle X-ray scattering (SAXS). GPS-NMR is used as a tool for fast analysis of the protein unfolding processes upon external perturbation, and DLS and SAXS are used for further structural characterization of the unfolding states. The combination allows addressing detergent properties and protein conformations at the same time. The mapping of the states reveals that KcsA undergoes a series of rearrangements which include expansion of the tetramer in several steps followed by dissociation into monomers at 29% TFE. Supplementary studies of DDM and TFE in the absence of KcsA suggest that the disintegration of the tetramer at 29% TFE is caused by TFE dissolving the surrounding DDM rim. Above 34% TFE, KcsA collapses to a new structure that is fully formed at 44% TFE.

1. Introduction

The integrity of membrane proteins within membranes is an intensely debated topic, which has stimulated the use of techniques as diverse as atomic force microscopy [1], laser-induced oxidation labeling [2], electrospray ionization mass spectrometry [3], Φ-value analysis [4], and molecular modeling [5], to provide information about the protein-membrane and intra-protein interactions stabilizing various folding states. Extensive studies, for example by the groups of Bowie[6,7], MacKenzie [8], Booth [4,9] and Otzen [10–13] have provided important information about folding, denaturation, and unfolding properties of helical membrane proteins, although details of these mechanisms are still subject to considerable debate. This is not unreasonable considering the challenge addressing not only the structures of the protein itself but also its environment, and the delicate interactions between these entities.

Insight into the so-called membrane folding problem, i.e., how membrane proteins fold in the membrane to reach their final topology [4,6] is essential for the understanding of misfolding processes that are involved in, among others, membrane protein recycling and human diseases. So far, the folding processes for β-barrel membrane proteins have been more extensively investigated and are better understood than for helical membrane proteins. This may be ascribed to the ability to refold such proteins directly from the completely unfolded denaturant-stabilized state into membranes or vesicles. Reversible unfolding have only been reported for a small collection of α-helical membrane proteins, including bacteriorhodopsin (bR) [14], diacyl glycerol kinase (DAGK) [15], disulfide bond forming protein B (DsbB) [11,12], and the potassium channel KcsA[16]. With regard to protein folding/unfolding, bR is probably the most well-characterized membrane protein [17]. For bR, a typical approach in unfolding studies has involved initial denaturation by SDS [18,19] followed by refolding by addition of bicelles containing a mixture

* Corresponding authors at: Center for Insoluble Protein Structures (inSPIN), Interdisciplinary Nanoscience Center (iNANO) and Department of Chemistry, Aarhus University, Langelandsgade 140, DK-8000 Aarhus C, Denmark. Tel.: +45 87155 913; fax: +45 8619 6199.
E-mail addresses: malmendal@sund.ku.dk (A. Malmendal), ncn@inano.au.dk (N.C. Nielsen).
[1] Present address: Instituto de Física, Universidade de São Paulo, Caixa Postal 66318, 05314-970 São Paulo, Brasil.

0005-2736/$ – see front matter © 2012 Elsevier B.V. All rights reserved.
doi:10.1016/j.bbamem.2012.04.005

of long- and short-chain lipids. The native state of bR is reached via a number of spectroscopically distinct intermediate states [20]. Interestingly, it has recently been observed that the SDS-unfolded state maintains most of the structure in the transmembrane core [2]. In a similar way, KcsA appears to preserve its tetrameric state also in the presence of harsh detergents like SDS [21]. KcsA has been studied using TFE as unfolding agent [16,22]. Unfolding of KcsA by TFE in similar settings has led to two different unfolding models. In the first model [23], TFE is proposed to indirectly affect KcsA stability by modifying the lateral pressure of the reconstituting lipid environment which depends on the nature of the molecule applied for the protein reconstitution, for example, whether KcsA is embedded in a phospholipid membrane or in a surfactant rim that solubilizes the protein [23,24]. In the second model [22], TFE is proposed to interact directly with the protein which subsequently rearranges and unfolds. The models agree in that dissociation and the unfolding of the tetramer occur at the same time, and in that the unfolding process goes through a stage where the helical content decreases.

With such complex interaction patterns, it is important to have available methods that quickly and with a reasonable amount of detail can map essential points for fundamental changes in the protein folding pattern as well as changes in the environment (unfolding/folding agents, membranes etc.) upon systematic change of system parameters. This may provide more information about distinct folding states and thereby underpin models describing the interaction of the denaturant with both the membrane protein and the lipid environment. To obtain simultaneous information about the unfolding process of α-helical membrane proteins as well as the involved changes in detergent and denaturant conditions, we explore here the use of the recent GPS-NMR (Global Protein folding State Mapping by NMR) technique [25] in combination with dynamic light scattering (DLS) and small-angle X-ray scattering (SAXS) to study TFE-induced unfolding of KcsA reconstituted in DDM rims. GPS-NMR offers the attractive feature of mapping all protons from the liquid-state NMR-visible constituents in the sample, including the protein as well as membrane/surfactant and denaturation agents. The use of principal component analysis (PCA), which is a data handling procedure not requiring detailed assignment of resonances, renders GPS-NMR an interesting complementary approach to existing high-throughput biophysical methods often only probing specific (e.g., fluorescently labeled) sites in the protein itself, global changes in the secondary structure, or the overall state of the system. On the basis of the combined information from GPS-NMR, DLS, and SAXS, we create links between models proposed from previous unfolding studies of KcsA and suggest a more general model for the main interactions involved in chemical unfolding of α-helical membrane proteins.

2. Materials and methods

2.1. Sample preparation

Expression of the wild-type KcsA protein with an added N-terminal hexahistidine tag in *Escherichia coli* M15 (pRep4) cells and its purification by affinity chromatography on a Ni^{2+}-NTA agarose column were carried out as reported previously [22]. We note that the KcsA (160 residues) used in this study has additionally a linker and six histidines leading to a molecular weight of 19.3 kDa for the monomer and 77 kDa for the tetramer [26]. For NMR experiments, titrations were performed on a solution of KcsA containing 5 mM DDM, 20 mM Hepes buffer, and 100 mM KCl at pH 7. The starting concentration of the protein was 1.3 mg/ml (16.8 μM in terms of KcsA tetramers) for NMR analysis. For SAXS and DLS, the same sample preparation and buffer were used with an initial protein concentration of 2.0 mg/ml (25.9 μM). For DLS experiments, the sample was diluted to an initial concentration of 0.38 mg/ml (5 μM) by the same buffer solution applied for the protein including 5 mM DDM. We note that SAXS modeling suggest that the DDM concentration was about 15 mM in the 2.0 mg/ml KcsA sample due to simultaneous up-concentration of protein and DDM during the preparation of the samples for SAXS (see Section 3.6). Based on these numbers, the initial concentration of free DDM in the DLS sample was 7 mM. For NMR, the solution also contained 10% D_2O for frequency lock and 0.25 mM sodium 2,2-dimethyl-2-silapentane-5-sulfonate (DSS) for chemical shift reference. The protein titrations were performed by adding TFE 0–50% (vol/vol) to a KcsA:DDM (1:300, KcsA tetramer:DDM monomer) solution in Hepes buffer (5 mM DDM, 20 mM Hepes buffer and 100 mM KCl at pH 7).

The titrations of DDM solutions (5 mM DDM, 20 mM Hepes buffer, and 100 mM KCl at pH 7) were performed under identical conditions with the exception that the DSS reference was included in a purpose-built glass microtube (1 mm in diameter) to avoid changes in the reference frequency due to potential interference due to interactions between DSS and TFE. All spectra were recorded at ambient temperature (298 K).

2.2. NMR experiments

KcsA 1D NMR spectra were acquired at 298 K on a Bruker Avance-II 700 widebore NMR spectrometer (700.09 MHz) (Bruker BioSpin, Rheinstetten, Germany) using a triple-resonance TXI probe equipped with a *z*-gradient. For each titration point a 1D ^1H NMR spectrum was acquired using a modified WATERGATE pulse sequence [27] with a selective pulse applied at 8 ppm to excite the relevant spectral region (32,768 points, 512 scans, spectral width of 17 ppm). 1D ^1H NMR spectra of DDM were obtained on a Bruker Avance-III 500 NMR spectrometer (500.13 MHz) using a triple resonance TXI probe equipped with a *z*-gradient. For each titration point a spectrum was acquired using standard WATERGATE [27] (9614 points, 64 scans, spectral width of 12 ppm). Prior to each acquisition, the sample was allowed to equilibrate for 5 min in the spectrometer, followed by quick shimming.

2.3. GPS-NMR analysis

Variations between spectra were analyzed by reducing the dimensionality of the data set using principal component analysis (PCA) [28]. The principal components (PCs) are uncorrelated, and ordered by the amount of information they contain. Each PC is described by a "loading" vector, that is, positive/negative resonances as a function of chemical shift, and "scores" that describe the relative contribution of the loading vector to each spectrum. The processes that occur, for example, as a ligand is added, are well described by a few PCs. Since the number of processes is much lower than the number of signals measured, this applies also in the case of severely overlapping resonances.

The data were Fourier transformed (FT) and apodized using TOPSPIN (Bruker BioSpin, Rheinstetten, Germany). An exponential line broadening of 5 Hz was applied to the free-induction decay (FID) prior to FT of the KcsA spectra. FIDs acquired from DDM samples did not require any line broadening. All spectra were referenced to DSS at 0.0 ppm, manually phased, and baseline corrected. Data reduction was accomplished by dividing the spectrum into 0.01-ppm regions (bins) over which the signal was integrated to obtain the signal intensity. For KcsA, only the region containing signals from the protein was used (11.0–5.8 ppm) for PCA, while for DDM signals from the hydrophobic chain were used. The signal intensity was normalized considering the volumetric dilution and the total signal intensity of the analyzed region. PCA was performed using Simca-P 12.0 (Umetrics, Umeå, Sweden). The number of significant PCs and the uncertainty in the score values were determined by cross-validation [29].

2.4. DLS experiments

Dynamic Light Scattering (DLS) was performed on an ALV system (ALV GmbH, Langen, Germany) operating at a wavelength of 633 nm and the scattered light was detected at an angle of 90°. All samples were centrifuged for 15 min at 4000 rpm prior to measurements. The TFE for titration was filtered to avoid introducing dust into the sample. For KcsA the sample was centrifuged after each TFE addition for TFE concentrations higher than 17% to sediment aggregates, as they became visible to the naked eye. The data were analyzed using the ALV Correlator 3.0 software by expressing the electric field correlation function as a sum of exponentials. The analysis was repeated using Origin (OriginLab) in order to obtain standard errors on the results. We note that with the use of the sum of exponentials, it was not possible to determine polydispersities for the individual components. The fits give the intensity-weighted diffusion constants, and the hydrodynamic (Stokes) radius R_h, was calculated using the Stokes–Einstein equation $R_h = k_B T/6\pi\eta D$, where D is the intensity-weighted translational diffusion constant, k_B Boltzmann's constant, T the temperature, and η the liquid viscosity. The values for the viscosities of the TFE–water mixtures were taken from Ref. [30]. For the samples with only DDM, two exponentials with diffusion constants corresponding to, respectively, 1–4 nm and 80–140 nm were required for fitting the correlation functions. For the DDM–KcsA samples, it was for some of the samples necessary to have one additional exponential. In this case the size of the smallest species was 1–8 nm, whereas the other components were in the range 22–500 nm. Only the results for the smaller species are given since it is this one that can be associated with, respectively, the DDM micelles in the DDM samples and with DDM micelles and DDM–KcsA complexes in the KcsA-containing samples.

The hydrodynamic radius (R_h) was calculated for the SAXS models using HYDROPRO [31,32] and for the ellipsoidal models for the DDM micelles it was estimated as the average outer radius as suggested in [33].

2.5. SAXS experiments

SAXS measurements were carried out on the laboratory-based small-angle X-ray scattering (SAXS) facility at Aarhus University [34]. The scattering data were collected for between 4 and 6 h, dependent on sample concentration, and so were their respective backgrounds. Initial data treatment, background subtractions, and conversion of the data to absolute scale, using water as a primary standard, were performed using the SUPERSAXS program package (Oliveira, C.L.P. and Pedersen, J.S., unpublished). Finally, the intensity, $I(q)$, was displayed as a function of the magnitude of the scattering vector, q. The scattering vector is given as $q = 4\pi \sin\theta/\lambda$, where the X-ray wavelength, λ, is 1.54 Å and 2θ is the angle between the incident and scattered X-rays. In order to obtain model-independent real-space information from the SAXS data an indirect Fourier transformation (ITF) [35] was performed for the data from the KcsA–DDM system. This procedure provides the pair distance distribution function, $p(r)$. The program WIFT [36,37] was used.

2.6. SAXS modeling

2.6.1. Micelle model

The SAXS data obtained for DDM micelles in 100 mM KCl with an increasing TFE concentration was modeled using an ellipsoid of revolution with a core–shell structure in which the thickness of the shell was constant. The scattering intensity can be expressed as $I(q) = nP(q)$, where n is the number density of particles and $P(q)$ the form factor. The two axes of an ellipsoid of revolution are related by the aspect ratio, ε. The orientationally averaged form factor for a core–shell structure is given by

$$P_e(q) = \int_0^{\pi/2} [\Delta\rho_{shell} V_{e,tot} \Phi(qr(R_e + D, \varepsilon_{shell}, \phi)) - (\Delta\rho_{shell} - \Delta\rho_{core}) V_{e,core} \Phi(qr(R_e, \varepsilon, \phi))]^2 \sin\phi d\phi,$$

using the normalized amplitude form factor $\Phi(qr) = 3[\sin(qr) - qr\cos(qr)]/(qr)$ and where $\Delta\rho_{shell}$ and $\Delta\rho_{core}$ are the excess scattering length density for the shell and core, respectively. The total and core volumes are given as $V_{e,tot} = (4\pi/3)(R_e + D)^2(\varepsilon R_e + D)$ and $V_{e,core} = (4\pi/3)\varepsilon R_e^3$, respectively. Further, $r(R_e, \varepsilon, \varphi) = R_e^2(\sin^2\varphi + \varepsilon^2 \cos^2\varphi)^{1/2}$ and φ is the angle between the scattering vector and the main axis of the ellipsoid. The head group layer has a constant shell thickness, D, which is obtained by $\varepsilon_{shell} = (\varepsilon R_e + D)/(R_e + D)$. The boundaries between the core and shell and the shell and solvent were made diffuse by multiplying the scattering amplitudes by $\exp(-\sigma^2 q^2/2)$, where σ is the width of the interface. The smeared interfaces are introduced as the boundaries are not expected to be sharp due to disorder on the molecular/atomic level. In the modeling D was fixed at 8 Å and the inner and outer interfaces (σ) were 1 and 3 Å, respectively. Aggregation numbers of the micelles are calculated by dividing the volume of the core of the micelles by that of a C12 hydrocarbon chain (352 Å^3) [38].

2.6.2. Models for protein–surfactant complexes

Modeling of the SAXS data was performed utilizing the known structure for KcsA for the Cα atoms (PDB: 1F6G). The excess scattering length of the points representing the Cα atoms was taken to represent that of an average residue. The detergent rim was modeled by Monte Carlo points to describe an ellipsoidal core–shell structure of a certain size with a constant head-group shell. The rim was placed to cover the hydrophobic transmembrane region of KcsA. Points in a volume within the ellipsoidal structure corresponding to that of the protein were discarded. The excess scattering length of the points within the hydrocarbon region and head-group region of the rim was taken so that the regions represent the scattering from a certain number of DDM molecules. When calculating the excess scattering length, the variation of the average electron density of the solvent when adding TFE was taken into account [30]. The theoretical scattering curve for the entire complex was computed using the Debye equation [39]. To account for free micelles in the solution a linear combination of the theoretical data from the model and scattering data obtained for free micelles was fitted to the experimental data.

3. Results

3.1. Mapping the interaction between KcsA and TFE using GPS-NMR

The interactions between TFE and KcsA reconstituted in DDM micelles in the presence of KCl were analyzed using GPS-NMR [25]. GPS-NMR combines the acquisition of simple/fast ^{1}H 1D NMR spectra during protein perturbation (e.g., by ligand titration) with PCA [40] to analyze spectral variation. This allows us to follow the overall spectral changes (in signal intensities, and line width) to describe the changes in the system during the titration. GPS-NMR is not limited to report on the total changes of the system but may also be focused on different regions of the 1D ^{1}H NMR spectra to follow the process of the individual constituents through selection of specific spectral regions.

Fig. 1a shows the series of ^{1}H NMR spectra recorded during a titration of KcsA in DDM with TFE using 12 min of acquisition after each addition of TFE (the total TFE concentration is marked on the spectra). To focus on the unfolding of KcsA, the GPS-NMR analysis (by PCA) was performed on the spectral region containing signals from amide and aromatic groups of KcsA, which also benefits from the absence of solvent signals (enlarged spectra of the spectrum region 5.5–10.5 ppm are reported in Fig. 3). Fig. 1a shows the spectral input to the PCA analysis, in this specific case a set of spectra where the

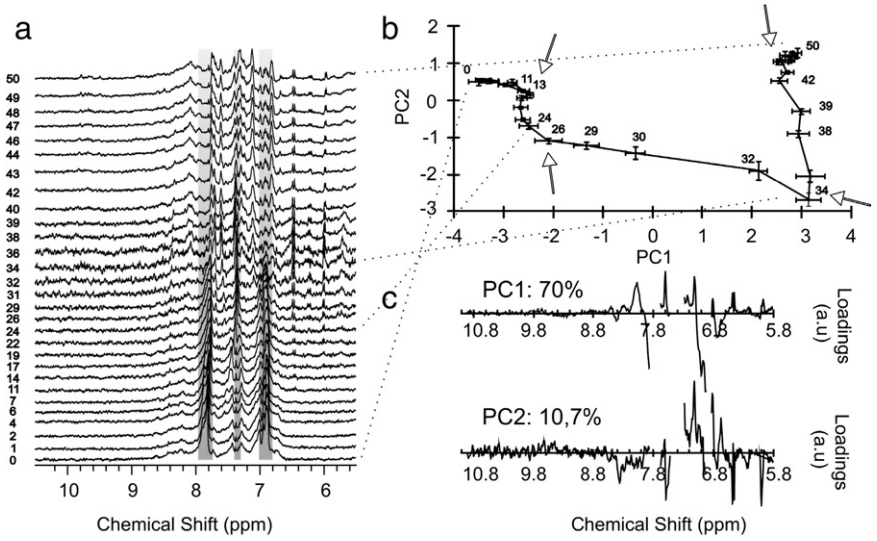

Fig. 1. GPS-NMR of KcsA–DDM complexes interacting with TFE. (a) The PCA input is represented by the original data (29 ^{1}H NMR spectra) normalized for the protein integral area. The shaded gray areas include ^{1}H NMR signals from the hexahistidine tag and are therefore not included in the PCA analysis. (b) 2D *PC1–PC2* score plot mapping the interaction of KcsA in DDM with TFE. (c) Loadings for the *PC1* and *PC2* principal components. TFE concentrations are marked in (a) and (b).

11.0–5.8 ppm region has been integrated into 520 bins of width 0.01 ppm normalized to the total integral area in the range 8.8–6.8 ppm. In Fig. 1a, the shaded gray areas mark the regions 7.52–7.29, 7.87–7.67 and 6.93–6.83 ppm which have been removed before the PCA to avoid potential interference from the hexahistidine tag HN, Hδ2, and Hε1 signals [41,42]. The analysis revealed three components accounting for 70, 11, and 5% (the total is 86%) of the spectral variation suggesting two intermediate states (three transitions). The 2D *PC1–PC2* plot in Fig. 1b provides a map of the interaction of TFE with KcsA reconstituted in DDM upon increasing the concentration of TFE over the range 0–50%, while the loadings for *PC1* and *PC2* included in Fig. 1c may provide details on the spectral components giving rise to the trajectory in the 2D score plot. *PC3* was not displayed since it accounts for a very limited fraction of the variation and does not improve the overall picture described by the *PC1–PC2* plot.

The 2D score plot (Fig. 1b) reveals an inflection at 34% but also a less sharp kink at 24–26% TFE and an end point at 44% TFE. These features are indicative of distinct folding states. Furthermore, the map indicates a possible additional intermediate state at 13% TFE (arrows, Fig. 1b). The state at 13% TFE is not accounted for by an additional *PC* (i.e., there is no fourth principal component), which might be because the changes below 13% are of relatively limited amplitude and/or are co-linear with the later changes. According to the map, *PC1* shows the greatest variation in two ranges, 0–13% and 24–34% TFE, particularly the latter region (see also Fig. 2a). *PC2* is mainly responsible for variation in the range 13–44% TFE. The loading plots in Fig. 1c show the relative contributions of spectral components at different chemical shifts to *PC1* and *PC2*. The positive and negative signals show how much the various components increase or decrease as the score increases (Fig. 1b and c).

Fig. 2 shows the GPS-NMR *PC1* and *PC2* scores plotted against the TFE concentration (Fig. 2a) along with the changes in the integral area of the protein ^{1}H NMR signals in the 6.8–8.8 ppm range (Fig. 2b), R_h measured by DLS (Fig. 2c), and the associated total light scattering intensity (Fig. 2d). Both *PC1* and *PC2* indicate a process with a turning point at 34% TFE. *PC1* increases with different rates, reaching a maximum rate between 29 and 34% TFE. Above 34% TFE, PC1 remains relatively constant. In the range 0–34% TFE, *PC2* decreases with an increasing rate and reaches a minimum value at 34% TFE, above this TFE concentration *PC2* increases reaching a value close to the original one at the final state around 44% TFE. The integral of the protein signals (Fig. 2b) also indicates that the TFE–KcsA interaction process is characterized by two main steps: one in which the signal decreases (0–34%) and a subsequent one in which the signal increases (34–50%). The signal decrease can be further split up into two regions: a gentle decline at 7–29% and then a sharper drop to an intensity close to half of the original at 34% TFE. The sharp decrease coincides with the region in which *PC1* reaches the maximum rate of change.

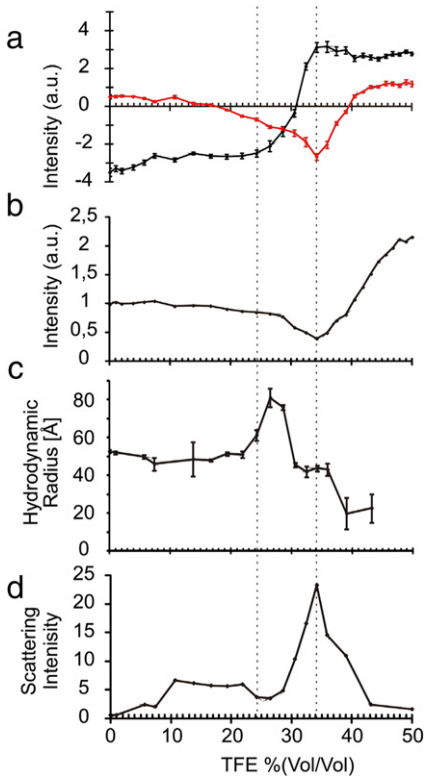

Fig. 2. Interaction of KcsA–DDM complexes and TFE probed using ^{1}H NMR and DLS data. (a) *PC1* (black) and *PC2* (red) principal components from the GPS-NMR analysis in Fig. 1. (b) Integral of the amide and aromatic ^{1}H NMR signals. (c) The number-average hydrodynamic radius of the particles in solution measured by DLS. (d) Intensity of the DLS signal. All parameters are shown as a function of the TFE concentration (vol/vol). All error bars represent standard errors. (For interpretation of the references to color in this figure legend, the reader is referred to the web version of this article.)

Comparison of the initial and final ^{1}H NMR integral areas (Fig. 2b) suggests that the native KcsA reconstituted in DDM is only partially visible by standard ^{1}H liquid-state NMR, probably due to the slow tumbling time of the KcsA–DDM complexes. It has been estimated that KcsA reconstituted in SDS has a molecular weight of 115 ± 10 kDa [43]; DDM has a higher aggregation number than SDS which likely corresponds to an even higher molecular weight of the DDM–KcsA complex as also revealed by the SAXS data (see Section 3.6). Most likely the NMR visible part of KcsA mainly corresponds to flexible regions of the protein including in particular the C-terminal domain [41,42]. The decrease in the NMR signal intensity around 34% TFE may be ascribed to various factors, including (*i*) precipitation (supported by the observation of white precipitate in the NMR tube in this concentration range of TFE, moreover precipitation has been previously reported for KcsA and other proteins under similar experimental conditions [10,23]), (*ii*) conformational exchange interfering with the NMR measurements, and (*iii*) slower tumbling time due to formation of increasingly sized KcsA–DDM–TFE complexes. Note the correlation between the decrease of the NMR signal and the *PC1* value in the range 24–34% TFE suggesting that the two variables are related. In contrast to the *PC*s, the intensity increases all the way up to 50% TFE, suggesting that it is only the concentration/dynamics and not the conformation of the protein that changes above 44% TFE.

3.2. Information from dynamic light scattering on KcsA–TFE interactions

In Fig. 2c, the R_h of the small species is displayed. It remains constant up to 17% TFE and then starts to increase in two steps: slightly between 19 and 22% TFE and more markedly between 22 and 29% TFE where it reaches a maximum. Notably, the R_h also suggests that most of the changes happen in the range of 24–34% TFE (the two concentrations marked with dotted vertical lines in Fig. 2. At 0% TFE, R_h is measured as 53 ± 1 Å, which is in agreement with the expected size of the KcsA tetramer [44] and the value calculated from the model derived from the SAXS data (see Section 3.6). However, it should be noted that the sample contains also a large amount of empty DDM micelles with R_h = 35.6 ± 0.2 Å as determined by DLS measurements on pure DDM solutions (see Section 3.5). Estimating the concentration of KcsA–DDM complexes and free micelles for aggregation numbers for DDM of, respectively, 250 and 120 (see Sections 3.6 and 3.5), it can be estimated that the contributions of the two species to the DLS intensity signal is about equal and therefore the determined R_h is an average of that of the complexes and the free micelles. The average R_h of the model for the complex and the free DDM micelle is estimated to be 44 Å which is somewhat lower than the experimental value. Up to a TFE concentration of 22%, the R_h is 46–51 Å. Estimating the average R_h for the SAXS model for the complexes and the free micelles at 22% gives a value of 40 Å also somewhat lower than the experimental value. The lack of change up to 22% TFE supports the limited changes in the GPS-NMR *PC1* and *PC2* components in this region. In the region of 24 to 29% TFE, the R_h reaches a maximum of 81 ± 5 Å. This large radius suggests that the protein forms a more extended structure here, coinciding with a major change in *PC1* in the GPS-NMR data. Since this large radius cannot be explained by a monomeric KcsA species, we suggest that KcsA still maintains a tetrameric form up to 29% TFE. Between 29 and 36% TFE, we observe a value of 44 ± 2 Å for R_h. The decrease in R_h, correlating with major changes in the GPS-NMR *PC2* component, is likely due to dissociation of the tetramer. This is in agreement with the findings that monomeric KcsA is detected from around 30% TFE by SDS-PAGE [22] and becomes accessible to chymotrypsin cleavage above 30% TFE. If monomeric KcsA is fully unfolded, R_h is expected to be 42 Å while it would be expected to have a radius of ~20 Å if folded to a plausible compact globular state [45]. The measured R_h of 44 ± 2 Å in the region 29 and 36% TFE may correspond to the presence of a fully unfolded monomer or a single monomer partially unfolded (see Section 3.3). Under experimental conditions identical to ours (5 mM DDM, 100 KCl and 20 mM Hepes), it has been observed that DPH (1,6-diphenyl-1,3,5-hexatriene) fluorescence is extinguished in the range around 30% TFE indicating a loss of micelles and KcsA-bound DDM [22]. In the same study, it was shown that the unfolding of KcsA takes place between 20 and 30% TFE. We note that the micelle disruption is confirmed by SAXS measurements performed during titration of DDM solutions (same detergent concentration and buffer) in the absence of protein. These measurements show that the DDM micelles are dissolved at about 22–24% TFE (see Section 3.5). Above 36% TFE, R_h decreases further to 21 ± 8 Å being in agreement with the expected radius of a compact globular state [45]. This suggests that in the absence of detergent molecules to protect the hydrophobic regions from contacts with the polar environment, the KcsA monomer loses its native structure and reaches a very compact (collapsed) folded conformation. This is in agreement with the finding that the folding process of KcsA is irreversible above 34% TFE [22]. The decrease of R_h between 36 and 50% TFE may be ascribed to a shift of the secondary structure towards a more α-helical state [46], potentially explaining the last step observed in the GPS-NMR 2D score plot in Fig. 1b revealing a change up to 44% TFE.

The light scattering intensity is proportional to *cM* where *c* is the mass concentration of the sample in the beam and *M* is the weight-averaged molecular mass of the particles. The light scattering intensity (Fig. 2d) can thus give additional information on the presence of aggregates in the sample, but the interpretation is not straightforward since it is also dependent on the concentration of soluble particles. The concentration of scattering objects was not constant as the samples above 17% TFE had aggregates and the samples were centrifuged to remove these [10]. Between 7 and 11% TFE, there is a good correspondence between the signal scattering increase and the slight NMR signal decay (Fig. 2b). Interestingly, the same concentration has been reported as the half transition point for the dissolution of KcsA clusters [16]. The data could indicate that dissolution of KcsA clusters results in a first weak precipitation process.

The volume fraction of aggregates at low TFE concentration is in agreement with the modeling of the SAXS data (see Section 3.6) which shows that all protein is in the complexes at 0 and 1% TFE. The appearance of large aggregates at 22% TFE in the SAXS data (see Section 3.6), and the fact that only about 50% of the protein is in the complexes, is also in agreement with the DLS intensity. Similar to the scattering intensity, the intensity of the ^{1}H NMR signals from the KcsA amide and aromatic regions increases with TFE concentration, but oppositely it decreases with an increasing particle size. Note that the particle size is described in terms of the local rotational correlation time, and thus describes the size of the independent structural units rather that of the whole particle. Qualitatively, changes in the DLS and NMR intensities have an inverse relation. But there are two important exceptions: there is no observable change in the NMR intensity corresponding to the increase in scattering intensity between 11 and 22% TFE; and in spite of the otherwise inverse relation, both intensities are higher at the end of the titration than in the beginning. This may suggest that the overall shape of the curve is dominated by changes in size and not concentration. It should be noted that even if the solutions used for NMR experiments were not centrifuged, aggregates of the size sensitive to centrifugation are not visible by NMR, and thus did not affect the NMR measurements as shown by a constant line width of the DSS reference signal (data not shown).

Above 25% TFE, the sedimented aggregates are redissolved resulting in a marked increase in the DLS signal intensity (Fig. 2d) until 33% TFE when the size of the aggregates starts to decrease strongly. This behavior correlates nicely with the changes in the GPS-NMR *PC1* component (Fig. 2a), the loss of NMR intensity (Fig. 2b), and the abrupt decrease of the R_h (Fig. 2c) in this region. All together, the data suggest that the tetramer after the expansion at 26–29% TFE dissociates,

which through formation of aggregates leads to increased precipitation. At 34% TFE, the scattering signal strongly decreases indicating a change of the main species in the solution in agreement with that the NMR signal intensity and the DLS R_h change significantly in the region above 36% TFE. Re-solvation of aggregates and perhaps even resolubilization of precipitates takes place at this high concentration of TFE.

3.3. ^{1}H NMR spectral signatures of folding states

To compare the spectral signatures of the different states discovered by GPS-NMR and supported by DLS measurements, ^{1}H NMR spectra observed for the KcsA:DDM:TFE mixture at 0, 24, 34, and 50% TFE are shown in Fig. 3. These spectra reflect the four main conformational states we are presumably operating with at this stage: the initial tetrameric state, a tetrameric state at 24% TFE, a monomeric state at 34% TFE and finally, a potentially refolded state at 50% TFE. Comparison of the spectra in Fig. 3a and b reveals changes in the dominant signals around 6.8, 7.4, and 7.8 ppm ascribed in part to signals from the hexahistidine tag. Disregarding these changes, the overall signatures of the spectra appear to be quite similar, implying that as viewed from the ^{1}H liquid-state NMR visible signals, the initial structure remains largely invariant, potentially with small changes as revealed by both the first and second principal component. SAXS data (Section 3.6) indicate a shrinkage of the DDM rim up till 22% TFE implying that new signals could appear due to the rearrangement of the protein (first denaturation) as the rim get smaller. Comparison of Fig. 3b and c reveals a more radical change of the overall spectrum, with the two broad resonances at 6.8 and 7.8 ppm in the 24% TFE spectrum being absent in the 34% TFE spectrum while the resolution of the observable protein signals increases. This is indicative of the introduction of new species that tumble faster, most likely being the KcsA monomer, while noting at the same time that the signal-to-noise ratio (cf. Fig. 2b) is lower due to simultaneous formation of larger aggregates. We note that at 34% TFE the signals are more dispersed, indicating a folded species in the solution in agreement with the R_h measurement. Comparison of the spectra at 34% (Fig. 3c) and 50% (Fig. 3d) TFE reveals that the further rearrangements occur in the 34–50% TFE region leading to higher signal intensities, sharper lines, and more chemical shift dispersion. At 9.8 ppm new signals appear in the spectrum which were assigned to Trp residues from the membrane–solvent interfacial regions of the helices not being visible at lower TFE concentrations. These well-resolved signals could be indicative of increased secondary structure of monomeric form refolding in the range of 34–50% TFE. This interpretation is corroborated by previous data [22] and by the well-known effect of TFE stabilizing α-helices [46,47]. The comparison of spectra in Fig. 3 and loadings in Fig. 1 suggests that *PC1* encapsulates aggregation and formation of a fast tumbling specie on going from 0 to 34% TFE.

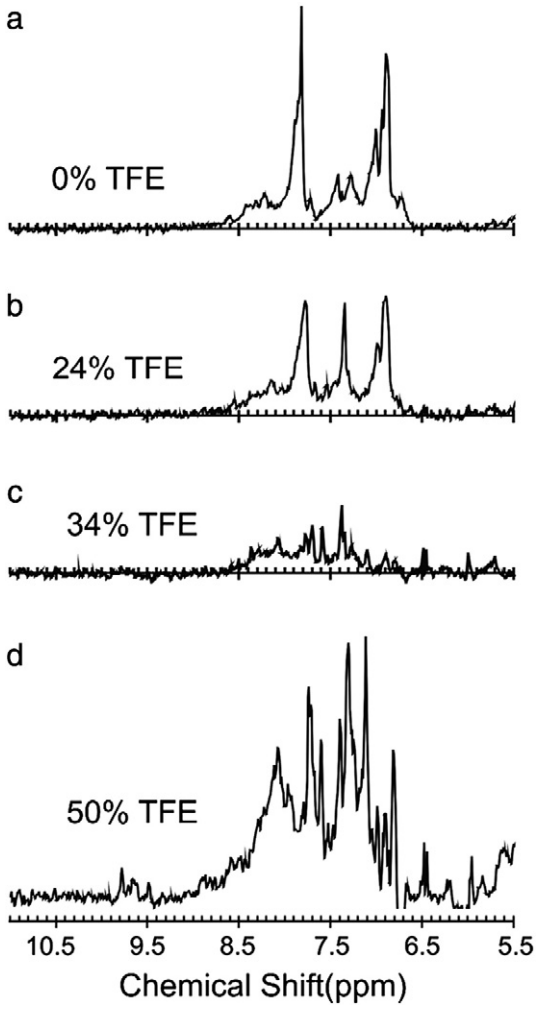

Fig. 3. ^{1}H NMR spectra displaying the region of amide and aromatic protein signals (11–5.5 ppm) for the KcsA:DDM complex in the presence of 0, 24, 34, and 50% TFE corresponding to the initial state, folding states identified by GPS NMR, and the final state. All spectra are normalized for gain and volumetric dilution to allow a direct comparison.

3.4. The effect of TFE: interaction between TFE and DDM in absence of KcsA studied by ^{1}H NMR

Understanding the behavior of TFE is a central ingredient in establishing a model for chemical unfolding of membrane proteins. The physical properties of TFE are known, and in the present context its clustering ability due to the hydrophobic trifluoromethyl group [48] is relevant. Cluster formation by TFE and other alcohols resembles micelle formation by surfactants to such a degree that the alcohol clustering concentration, ACC, has been introduced to describe the phenomenon [49]. TFE affects protein structures by increasing the strength of hydrogen bonding and charge–charge interactions, and decreasing the hydrophobic effect [47,50]. The interaction between membrane proteins and TFE is anticipated to follow similar trends as for soluble proteins where two major effects are observed: (*i*) TFE penetrates the hydrophobic core and solvates certain groups in the polypeptide chain. This structural destabilization causes formation of aggregates or in some cases even fibrillar structures [51] below 35% TFE with the lower concentration limit depending on the stability of the protein [52]. (*ii*) At higher TFE concentrations the increase in hydrogen bond strength stabilizes helical structures [47,53] which has been observed for KcsA in the interval between 35 and 55% TFE [22].

For membrane proteins, the interactions between TFE and the membrane or the membrane-mimicking detergents are also of importance. The buildup of a new structure for KcsA in DDM micelles in the region between 34 and 50% TFE may be due to the stabilization of α-helices as observed for soluble proteins [46]. Similarly, formation of precipitate is in agreement with the findings for soluble proteins, but it is not obvious that it is only the direct KcsA–TFE interactions that are important for the tetramer stability. As an example, the gradual addition of TFE to a solution of DDM changes the overall physico-chemical properties of the detergent system, including the critical micelle concentration (CMC) of DDM [54]. Accordingly, the perturbation of DDM by TFE may indirectly induce structural changes in KcsA as part of the three-component system KcsA:DDM:TFE. Further evidence for this is provided by stopped-flow studies in which changes in the kinetics of unfolding coincide with changes in TFE–DDM interactions (see Supplementary information).

To shed further light on the complex interactions in the KcsA:DDM:TFE system, we supplemented our GPS-NMR analysis with an investigation of the interaction of TFE with DDM micelles in the

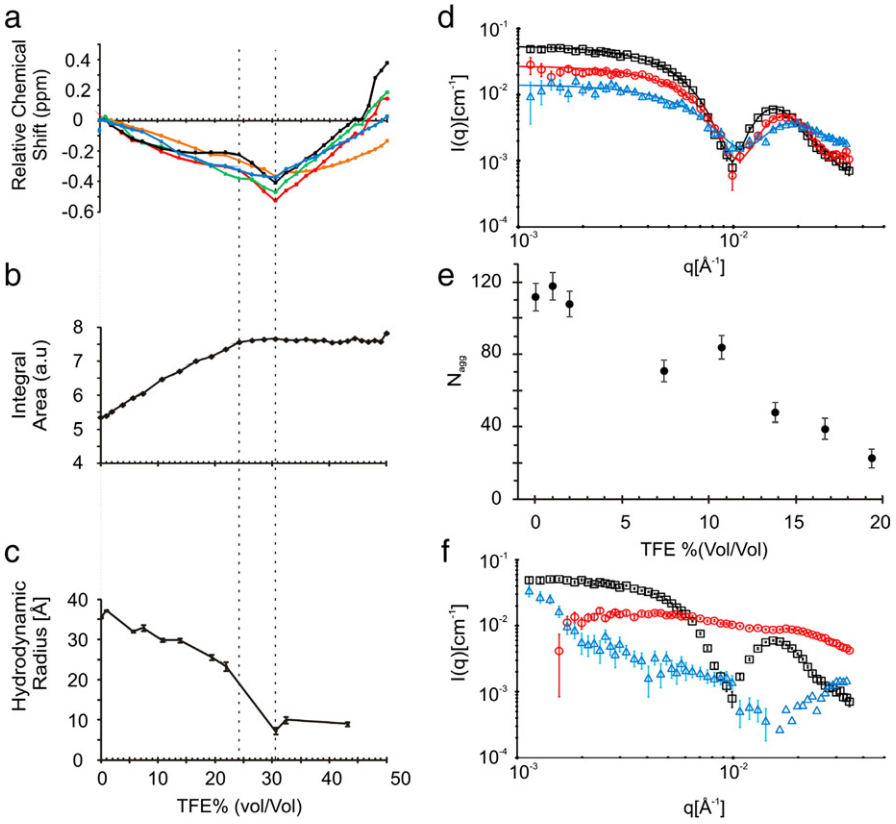

Fig. 4. Interaction of TFE with DDM micelles. (a) Comparison of the ^{1}H chemical shift variation for various protons: DDM CH_3 (black line), DDM CH_2(3–11) (red line), DDM CH_2(2) (green line), DDM anomeric proton (blue line), and TFE protons (orange line). Numbers in parenthesis indicate the position of the proton on the DDM aliphatic chain. (b) Intensity (integral area) of the DDM CH_2(3–11) signal. (c) Number average hydrodynamic radius of the particles in solution as probed by DLS. (a–c) are reported as a function of the TFE concentration (vol/vol). (d–f) SAXS data. (d) Scattering data for DDM without (black squares), with 7% (red circles), and 17% (blue triangles) TFE and their corresponding model fits using a core–shell ellipsoidal model, black, red and blue solid lines, respectively. (e) Micellar aggregation numbers calculated from core volume obtained from the modeling. (f) Scattering data from DDM in the presence of 0 (black squares), 22 (red circles), and 32% (blue triangles) TFE. (For interpretation of the references to color in this figure legend, the reader is referred to the web version of this article.)

absence of KcsA by ^{1}H NMR, DLS, and SAXS measurements as summarized in Fig. 4. Addressing first the ^{1}H NMR measurements, TFE and DDM display a few sharp signals well distributed over the ^{1}H chemical shift region, wherefore we resort to standard data analysis rather than PCA in this case. The experiments were conducted by adding TFE to a solution of 5 mM DDM in 100 mM KCl, after which 1D ^{1}H NMR spectra were recorded and the chemical shifts for the TFE and DDM constituents measured. For DDM, we measured chemical shifts of the anomeric proton of the hydrophilic sugar head and the hydrophobic tail protons: CH_2(2) close to the DDM sugar rings, CH_2(3–11) in the middle of the chain, and CH_3 at the end (numbers in parenthesis denote carbon position). For comparison, the chemical shift changes relative to the relevant chemical shift observed prior to addition of TFE ($\delta - \delta_0$) are shown in Fig. 4a. The chemical shifts of all signals decrease until 31% TFE and then increase again. Addition of TFE affects the dipolarity, acidity, and basicity of the water/TFE solution [55]. Interestingly, the systematic chemical shift changes are consistent with the changes in basicity, that is, the ability of the solvent molecules to function as hydrogen-bond donors, as measured previously for TFE/water mixtures [55], which increases up to 31% TFE and then decreases.

A more detailed look at the ^{1}H chemical shifts reveals that the shifts of the anomeric (Fig. 4a, blue line) and CH_2(2) (Fig. 4a, green line) protons decrease almost linearly up to 31% TFE. The CH_2(3–11) (Fig. 4a, red line) and CH_3 (Fig. 4a, black line) protons in the DDM tail are affected differently, which was ascribed to shielding from the solvent by the micelle. Consequently, this effect is most pronounced for the CH_3, which is considered most deeply buried in the micelles. An effect of TFE is to decrease the solvent polarizability [55], and it has been shown that the CMC increases as the solvent polarizability decreases [54]. The smaller shift changes for the CH_3 up to 24% TFE are consistent with a model where these protons are still solvent protected by DDM molecules rearranging to form micelles of smaller and smaller dimension until they finally form small aggregates of 2–3 molecules earlier referred to as premicelles [56]. All DDM protons reach their lowest chemical shifts around 31% TFE. Fig. 4b shows the intensity of the DDM CH_2(3–11) ^{1}H NMR signals, that constantly increases up to 24% after which it stays constant. This was ascribed to a higher degree of mobility of DDM molecules (within the micelle, exchange of molecules in and out of the micelle, or of the entire micelle) and/or a higher population of DDM molecules in a liquid-state NMR-visible state. Up to 31% TFE, the shape of the intensity curve resembles that for the anomeric ^{1}H chemical shift (except for the sign), suggesting that the two parameters depend on the same environmental factors. The observations are consistent with DDM molecules assembling into smaller micelles or being released as monomers up to 24% TFE. This concentration corresponds to the end of the plateau described by the chemical shift of the CH_3. The sharp decrease in the chemical shifts for CH_2(3–11) and CH_3 up to 31% TFE likely describes an increase in TFE exposure in this range. As judged from the CH_2(3–11) signal intensity, this exposure is not related to the type of mobility described by this parameter.

3.5. DLS and SAXS analysis of DDM–TFE complexes

The DLS data for DDM titrated with increasing amounts of TFE (Fig. 4c) show a decreasing micelle size as measured in terms of the R_h. At 31% TFE, R_h is very small (10 ± 1 Å) which is ascribed to DDM

being present in a monomeric form. Interestingly, the dissolution of the micelles at 31% TFE coincides with the maximum value for the TFE basicity that was also reflected in the chemical shifts of DDM and TFE.

SAXS data for DDM micelles with an increasing TFE concentration are reported in Fig. 4d–f. The data below 20% TFE display a pronounced minimum and a secondary maximum at higher q, which is characteristic for core–shell micelles with an opposite sign of the excess electron density in the core and shell. For hydrocarbon micelle cores in water, the electron density is lower than that of water giving a negative excess electron density. The polar head groups are more electron dense and have a positive excess electron density in water. The data were analyzed by fitting an elliptical core–shell model to the data. For 0–2% TFE, oblate shaped micelles give the best fits to the data, whereas the fits are equally good for oblate and prolate shaped micelles for larger TFE concentrations. The model does not fit the data satisfactory above 19% TFE. The aggregation numbers and hydrodynamic (see Section 2.6) radii derived from the oblate and prolate models are similar, and only the results for oblates are given in the following. A subset of the SAXS data with their respective fits is shown in Fig. 4d, (for further explanation, see Materials and methods). At TFE concentrations between 0 and 2%, the micelles have an aggregation number N_{agg} of around 110–120 (Fig. 4e), similar to earlier reported values [38,57,58]. Gradually increasing the TFE concentration decreases the micelle size and thus the aggregation number, as shown in Fig. 4e. The decrease in micellar size is in agreement with the observations from DLS. For the SAXS data at 0% TFE, the model has micelle core half axes of (25.9 ± 0.2 Å, 25.9 ± 0.2 Å, 13.9 ± 0.2 Å) and a fixed headgroup shell thickness of 8 Å. The dimensions of the core change gradually to (19.4 ± 0.5 Å, 19.4 ± 0.5 Å, 10.8 ± 1.0 Å) at 14% TFE. Upon addition of TFE to the system the micellar size decreased further.

The R_h of the micelles was also calculated from the micelle model determined by SAXS. The calculation uses the micelle dimensions [33] and considers also the roughness of the outer interface by adding two times the width of the interface to the size. The value is 33 Å at 0% TFE and decreases linearly to 25 Å at 19% TFE in very good agreement with the experimentally determined values (Fig. 4c)

Increasing the TFE concentration to 22–24% introduces a significant change in the SAXS scattering pattern, (Fig. 4f). The signature of a core–shell particle vanishes, however, the data clearly show the presence of variation in electron density on the nanometer length scale. Thus, micelles in the normal sense are no longer present in the solution. However, the surfactant is not dissolved as single molecules. At TFE concentrations of 31% and above, the scattering resembles that of small molecules. Accordingly, it is expected that the DDM molecules are present as single molecules in the solution at these concentrations of TFE. This is in agreement with the DLS measurements where the R_h from 31% and above is very small, around 10 Å. As discussed below the change in the level of surfactant organization occurring between 24 and 31% TFE has the interesting characteristic that it causes a sharp decrease in the ^{1}H chemical shifts for CH_2(3–11) and CH_3 while leaving that of the anomeric proton largely unaltered, implying that the chemical environment of the detergent tails changes drastically while it remains unaltered in the heads.

Goto et al. previously reported alcohol clustering of TFE in water [49]. We also collected SAXS data on the TFE–water mixtures (data not shown), which indicates that small clusters are present for TFE concentrations above 20% TFE, however, with a correlation length that does not exceed 5 Å. This cluster size is obtained from the SAXS data for the TFE–water mixtures by fitting a Lorentzian function. Between 31 and 47% TFE, the ^{1}H chemical shifts of all the tail protons are similarly affected (Fig. 4a). However, above 47% TFE a possible interaction between CH_3, which is the most hydrophobic part of the molecule, and these clusters might be suggested by the sharp increase in the CH_3 chemical shift (Fig. 4a, black line), which is not seen for the rest of the molecule at these concentrations.

Overall, our data suggest that the interaction between TFE and DDM can be described by two phases: micellar shrinkage and TFE cluster formation. In the first phase, TFE makes the DDM molecules rearrange to form micelles of gradually decreasing size. At 22% TFE there are no more micelles in the solution leaving clusters of a few molecules (premicelles) and around 31% TFE, DDM is monomeric in the solution. After that TFE molecules rearrange to form small clusters. This observation has implications on our interpretation of the KcsA data in the sense that it may suggest that the disassembly of the tetramer at 29% TFE is caused by TFE dissolving the surrounding rim, and that the collapse of the KcsA structure is caused by dissolution of all DDM molecules by TFE. However, the unfolding of the solvent exposed domains of KcsA around 24% TFE cannot be explained by the interactions between DDM and TFE, and is likely due to direct interactions between TFE and the protein as discussed above.

3.6. SAXS measurements on KcsA–DDM complexes influenced by TFE

With the aim of obtaining more information about the structure of KcsA solubilized by DDM and the influence of TFE, we performed SAXS measurements on the KcsA–DDM system in the presence of 0, 1, 22, and 29% TFE. Those values were chosen to verify the effect of

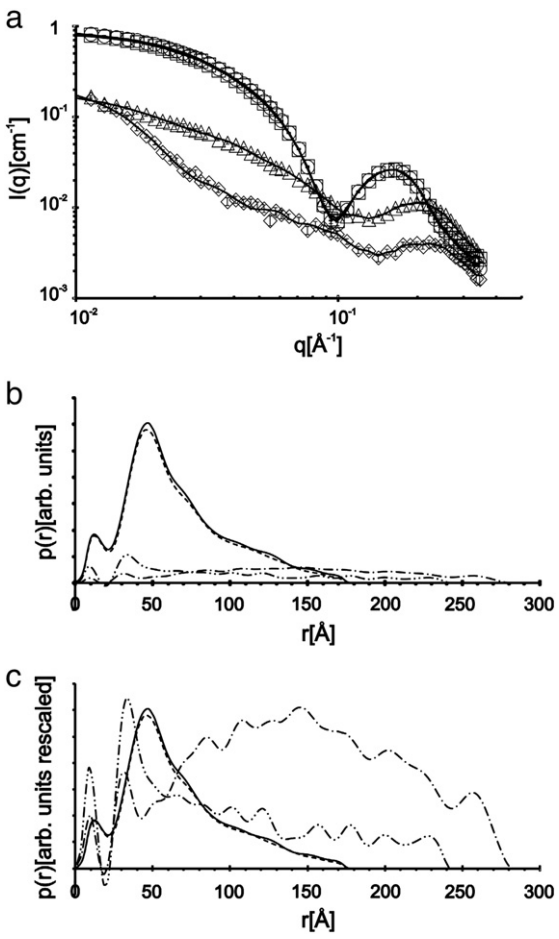

Fig. 5. Influence of TFE on the KcsA–DDM system investigated by SAXS measurements. (a) Intensity of the scattered signal, $I(q)$, is reported at 0 (squares), 1 (circles), 22 (triangles), and 29 (rhombus) % TFE (v/v). The full lines are fits from the indirect Fourier transformation. (b) The pair distance distribution function, $p(r)$, obtained from the indirect Fourier transformation of the scattering data in (a). Solid (——), dashed (– – –), double dotted-dashed (–··–) and, single dotted-dashed lines (–·–) represent 0, 1, 22 and 29% TFE, respectively. (c) The pair distance distribution function, $p(r)$, as in (b) but rescaled.

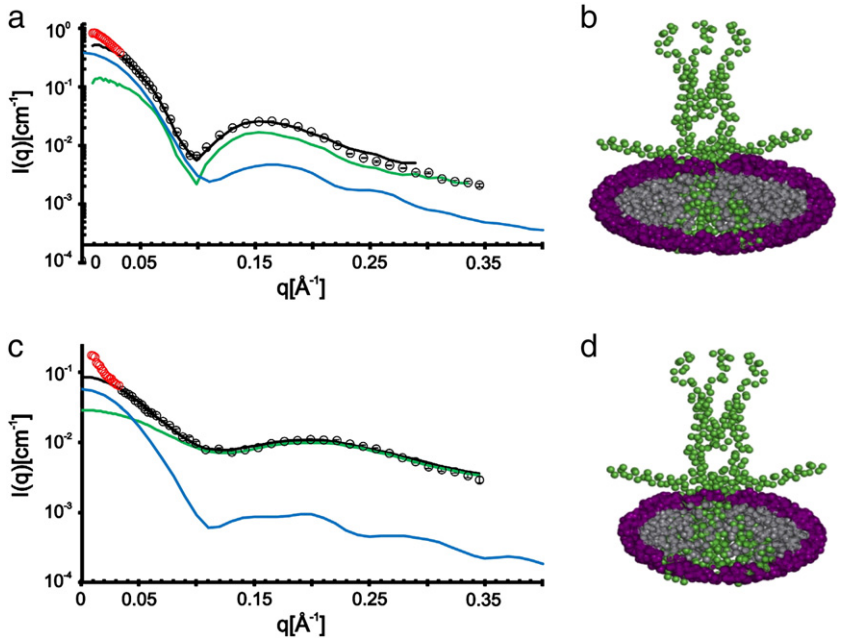

Fig. 6. (a) SAXS data for KcsA–detergent without TFE (circle) and corresponding model fit (black line), model scattering from protein–detergent complex (blue line) and SAXS from free DDM micelles (green line). Red points in the scattering data below 0.04 $Å^{-1}$ were not included in the modeling. (b) Model of KcsA with detergent rim of 250 DDM molecules based on the model of the protein without TFE [45]. The front part of the structure is cut away to allow a better view of the core–shell structure of the rim. The rim model has a hydrocarbon core with a half thickness of 15 Å close to the protein. The rim core has a radius of 43 Å in the perpendicular direction measured from the center of the protein to the edge of the rim core. The surfactant headgroup shell thickness is 8 Å. (c) SAXS data for KcsA–detergent in 22% TFE (circle) and corresponding model fit. The signatures are the same as in (a). (d) Model of KcsA with a detergent rim of 150 DDM molecules used in the modeling of the protein with 22% TFE. The hydrocarbon core of the model has, as for 0% TFE, a half thickness of 15 Å close to the protein, whereas the radius of the rim core is 36 Å. The headgroup shell thickness is also 8 Å for this model. The same KcsA structure [45] is used in the two models.

TFE at very low concentration (0 and 1% TFE) and to compare the aggregation state of DDM molecules with and without the protein (around 22–24% TFE, it is expected that DDM micelles dissolve in the absence of protein). The data are shown in Fig. 5a and the corresponding $p(r)$ obtained by IFT are shown in Fig. 5b and c. The SAXS data show a minimum and a clear secondary maximum at high q, similar to what is observed for the pure DDM micelles in the TFE mixtures. The secondary maximum also moves to higher q values with increasing amounts of TFE. This shows that core–shell structures are also present in the samples with KcsA. The $p(r)$ function corresponds to a histogram of distances between pairs of points within the complexes weighted by the excess electron density at the points and it has been normalized for the variation in protein concentration resulting from the titration with TFE. The oscillatory feature at short distances in $p(r)$ originates from the core–shell structure of the DDM rim and the DDM free micelles and the variation of excess scattering length between surfactant tail and head. Overall, there is a large variation in the shape and scale of the $p(r)$ functions in Fig. 5b. The contrast of the protein is reduced between 0 and 29% TFE from about 0.10 to 0.06 e/$Å^3$, however, this is not enough to explain the changes. Therefore one has to conclude that protein is precipitating and not contributing to the SAXS signal at 22 and 29% TFE consistent with the DLS data in Fig. 2. Another important parameter that can be derived from the $p(r)$ functions is the maximum diameter of the complexes. It is 175 Å for 0 and 1% TFE and, respectively, 240 Å and 280 Å for 22 and 29% TFE. These values are much larger than the corresponding value of about 116 Å that can be derived from the structure of the KcsA tetramer [44]. This shows that even for 0 and 1% TFE, the complexes tend to associate which could explain the higher observed hydrodynamic radii compared to those estimated for the samples containing both complexes and free DDM micelles. The presence of aggregates and clusters can also be directly observed in the SAXS data, in particular for 22 and 29% TFE as the strong increase in intensity as q goes towards zero. KcsA is known to form clusters [16,59], however, we cannot from the data conclude anything about the structure of these aggregates. In order to reduce the influence of the clusters in the further modeling data below $q = 0.04$ $Å^{-1}$ was disregarded.

A structural model (Fig. 6b) for the KcsA–DDM complex was constructed using the structure of KcsA (PDB entry: 1F6G) [44] for the Cα chains and a detergent rim represented by points generated by Monte Carlo methods. When comparing the scattering from the model to the SAXS data, the scattering from free DDM micelles corresponding to 5 mM DDM was added. However, this did not give a satisfactory fit to the data since the secondary maximum is more pronounced than this combination gives. The KcsA was up-concentrated to about 2.0 mg/ml for the SAXS measurements, and in this process there is a risk of also up-concentrating the DDM. Therefore, we also considered the possibility of having a larger concentration of DDM. The best fit of the model was obtained when adding the scattering from free DDM micelles corresponding to three times the expected concentration. Note that the scattering for free micelles at this concentration was measured independently for the relevant TFE concentrations. Although the micelles dissociate above a TFE concentration of 20% at 5 mM DDM, a 15 mM DDM sample has a concentration above CMC and micelles are still present at this concentration.

Without TFE, a model of KcsA with a detergent rim of 250 DDM molecules and a free micelle concentration of 15 mM describes the SAXS data. The model fit (Fig. 6a) yields a reduced χ^2 value of 51 (with the dominating contribution from deviations at high q) so the fit is not perfect, however, as the figure shows, the modeling of the data reproduces quite well the q dependence of the SAXS data, with the largest deviations at large q. This allows us to conclude that the model displayed in Fig. 6b is a very likely model for the complexes in the absence of TFE. The scattering intensity of the model is in good agreement with the SAXS data on absolute scale and we estimate that 90–100% of the protein is in the solution. The dimensions of the rim in the model are given in the caption of Fig. 6b. The R_h of the model for the KcsA–DDM complex was calculated as 51.1 Å using HYDROPRO [31,32]. The comparison of this value to the experimentally determined value requires the consideration of the free

micelles as described above. The SAXS data at 1% TFE is very similar to those in pure water and therefore these data were not modeled.

The SAXS data of the KcsA–DDM system were also modeled at 22% TFE (Fig. 6c and d). This was possible by assigning a smaller DDM rim of 150 molecules to the complex and by combining the scattering of the complex with that of DDM micelles in 22% TFE and 15 mM of DDM. The model fit yields a reduced χ^2 value of 5 and it is evident that there are still free micelles in the solution. The dimensions of the rim are given in the caption of Fig. 6d. The R_h calculated by HYDROPRO [32] is 46.5 Å.

The modeling shows that it is possible to describe the experimental SAXS data sets at both 0 and 22% TFE with the same structure of KcsA, however, assigning a smaller DDM rim to the protein at 22% TFE. This is in agreement with the CD measurements [22] which show that the secondary structure of KcsA is preserved up to 22% TFE. Comparing the scattering intensity of the model with the SAXS data on absolute scale allows us to estimate that about 50% of the protein is in the complexes at 22% TFE. The SAXS data at 29% TFE and the $p(r)$ function suggest that the KcsA structure is open with long intra-complex distances. At high q, the data follow the scattering from empty micelles, and at low q, there is an additional contribution from larger structures. The data thus contain very little information on the structure of KcsA and therefore these data were not modeled. These findings are all in good agreement with the GPS-NMR and DLS results and their interpretations as discussed above.

4. Discussion

The interaction of TFE with an α-helical membrane protein, KcsA, has been investigated by GPS-NMR and measurements of other NMR

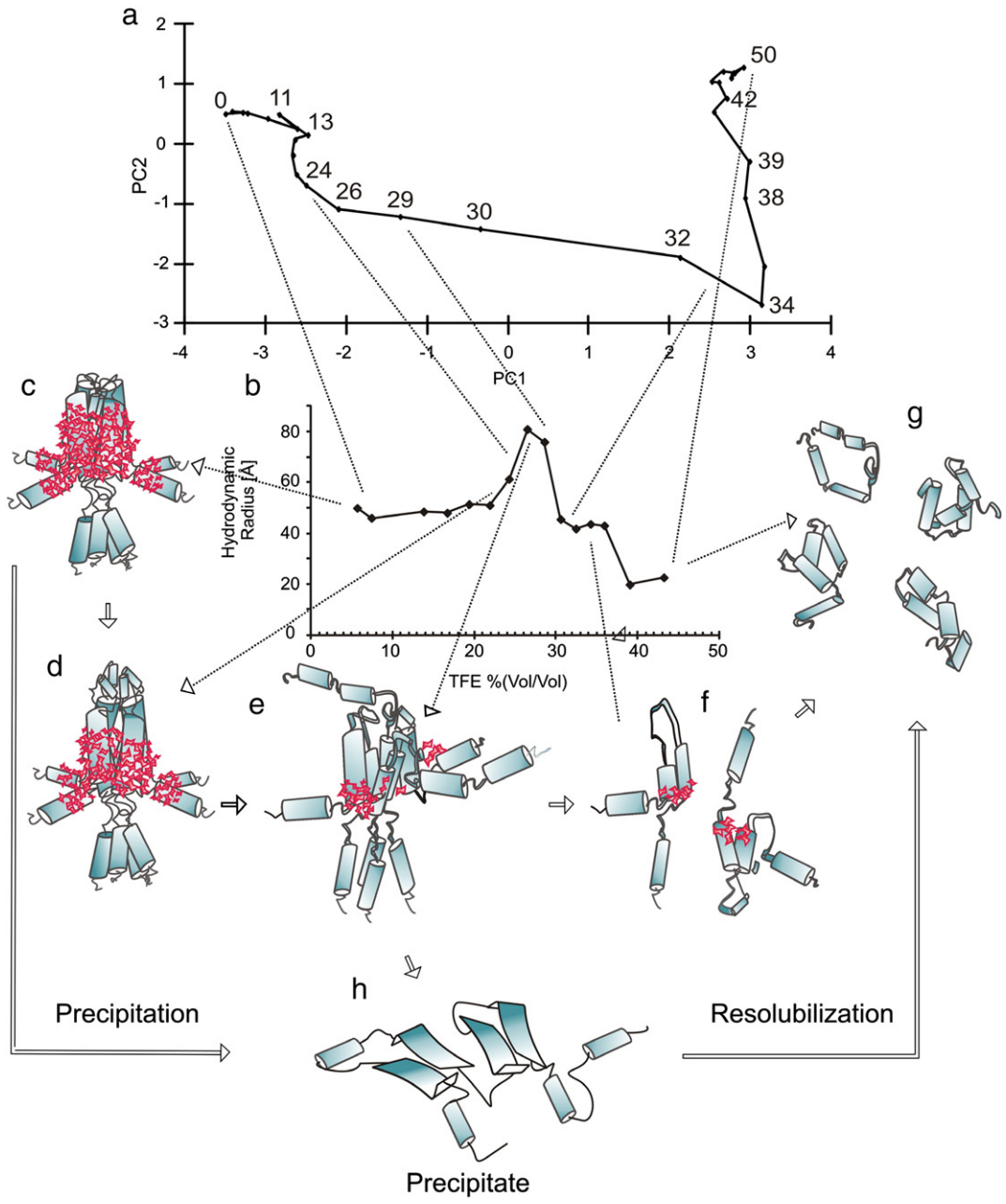

Fig. 7. Model for TFE induced unfolding of KcsA in DDM micelles based on GPS NMR, DLS, and SAXS experiments. In the middle of the figure selected parts of (a) GPS-NMR and (b) DLS data summarize the main steps involved in the interaction of TFE with KcsA. Dotted lines between panels (a) and (b) indicate the initial (0%), the turning points (22 and 34%) and the final conformational state of KcsA as discovered by both GPS-NMR and DLS data. Cartoons in (c–g) show a model of the conformational changes of KcsA as DDM is displaced. The panels c–g represent KcsA at 0, 22, 29, 34 and 44% TFE (v/v), respectively, while panel h illustrates the precipitate.

parameters, DLS, and SAXS. GPS-NMR is a new method which here is applied to give an overview of the folding space of KcsA. To summarize the results of our measurements and the data reported in the literature [16,22–24,43,60], the model in Fig. 7 is proposed for the interaction of TFE with KcsA reconstituted in DDM micelles.

In Fig. 7a and b, the GPS-NMR 2D score plot and the DLS data are reported along with schematic illustrations of the different states populated by KcsA at increasing TFE concentrations (Fig. 7c–g). The native structure in Fig. 7c is based on the architecture of full length KcsA [44] and displayed in accordance with the SAXS model discussed above. According to GPS-NMR and SAXS, the main changes up to 24% TFE are due to the shrinkage of the rim surrounding the protein, which represents a first rearrangement in the protein. The cartoon presented in Fig. 7d shows an exposed turret, but the denaturation could also involve a rearrangement of the soluble C-terminal. This KcsA state is based on the model by de Kruijff and coworkers [24] and is in agreement with the SAXS model at this TFE concentration. The decrease of the protein signal intensity measured by ^{1}H NMR (also supported by DLS and SAXS observations), which could be due to the formation of precipitate [23] is represented in the model by the β-sheet aggregates (Fig. 7h). The β-conformation is consistent with experimental results from the groups of de Kruijff [23] and Otzen [10,23]. Above 22–24% TFE, KcsA starts to rearrange to an expanded form (Fig. 7e) as also revealed by CD [22] and DLS measurements. There are several possible ways in which the tetrameric form may expand or dissociate. DDM molecules and TFE could accumulate around the protein forming a very large soluble aggregate. The tetramer could alternatively dissociates into two KcsA dimers which move away from each other as the TFE concentration is increased. An open tetramer with a smaller number of DDM molecules associated seems to be consistent with the previous gradual displacement of DDM and with the later stages of the model. In fact, the open tetramer explains the abrupt formation of the monomer, the large R_h measured by DLS, and the formation of a partially folded monomer above 29% TFE. The tetramer breaking could also lead to precipitation as reported by the decrease in the overall ^{1}H NMR signal intensity and previous data [23]. The small arrow (Fig. 7h) indicates further precipitation. Between 29 and 34% TFE, the main species in the solution is a semi-folded monomer as judged from the NMR spectra, DLS, CD data, and by chymotrypsin data [23] (Fig. 7f). ^{1}H NMR and DLS also suggest resolubilization of precipitated protein in accordance with earlier observations for DsbB [10]. The solvent exposed parts of the protein are unfolded before and during dissociation of the tetramer. Above 34% TFE the displacement of the last DDM molecules results in the formation of a collapsed monomer (Fig. 7g), and the structural information transmitted by the translocon during the native folding process is permanently lost. Returning to TFE concentrations lower than 34% is not sufficient to reconstitute the tetramer [22]. The irreversible collapse above 34% TFE helps us understand that temperature-induced unfolding of α-helical membrane proteins is irreversible because the detergent molecules are irreversibly displaced by the increase in kinetic energy at higher temperatures. The collapsed monomer structure is fully stabilized at 44% TFE.

The model in Fig. 7 is consistent with earlier experimental results. First of all, the reversibility of the process up to 34% [22] could be due to the formation of a partially unfolded monomer that can reconstitute the tetramer after dilution as the transmembrane segments are not yet irreversibly collapsed. At the same time, the model explains why the monomeric form of KcsA is the most prevalent at higher TFE concentrations [22]. Both direct and indirect interactions between TFE and KcsA are central in the model. The high hydrophobicity of TFE could be responsible for the interactions with both the detergent and hydrophobic regions of the protein. Up to 22–24% TFE, the main changes are in the detergent rim of the protein, and above 22–24% TFE in the protein structure. As indicated by previous models, denaturation and tetramer dissociation are coupled processes [22,23]. Barrera et al. has shown that in the range 1–50 mM DDM the $TFE_{1/2}$ needed to unfold the protein does not change with the DDM concentration [22]. Van den Brink-van der Laan have suggested that the effect of TFE on KcsA depends on the effective overall shape of the lipids applied to the protein reconstitution [23]. By considering the possibility that KcsA and detergent molecules could form independent particles with properties different from those of the coexisting pure DDM micelles, it remains unclear if the direct interaction of TFE with the protein or the DDM displacement is responsible for the protein denaturation. The retention of secondary structure even above 30% TFE as indicated by the NMR spectra (see Section 3.3) may indicate that the most of the unfolding involves soluble regions of KcsA (for example the turret region as previously suggested [24]). On the contrary, α-helical regions which strongly interact with lipids [60] and are naturally embedded in the membrane could preserve their structure up to the definitive displacement of DDM molecules. Therefore, the actual extent of unfolding of KcsA induced by TFE is not yet known and requires further investigations.

From a biological point of view the model shows the indispensability of the membranous environment during the folding or refolding of membrane proteins. It has been shown that KcsA requires some lipids bound to allow refolding [60]. The translocon is thus necessary to drive the interaction between the folding helical membrane protein and the lipid.

A better understanding and conciliation of the data previously produced by different techniques (among these UV and CD spectroscopy, chymotrypsin digestion and differential sedimentation) regarding folding and unfolding of KcsA has been here achieved and expressed by the presentation of a low-resolution unfolding model. Such a model takes into account direct and indirect interactions of TFE with KcsA protein but also interactions of TFE with the detergent molecules. The model is obtained owing to the combination of SAXS, DLS, and GPS-NMR methods. The experimental approach is specifically applied to KcsA reconstituted in DDM but it can be applied to any membrane protein and is a powerful way to investigate membrane protein folding and unfolding processes. Even though the model is of low resolution, the strategy presented here allows fast mapping of global changes in complex systems and the identification of transition points in the systems.

Acknowledgements

We acknowledge support from the Danish National Research Foundation and The Danish Council for Independent Research Natural Sciences. Support by grants from the Spanish DGI BFU2011-25920 and Consolider-Ingenio 2010 CSD2-2008-00005 is also acknowledged.

Appendix A. Supplementary data

Supplementary data to this article can be found online at http://dx.doi.org/10.1016/j.bbamem.2012.04.005.

References

[1] J. Preiner, H. Janovjak, C. Rankl, H. Knaus, D.A. Cisneros, A. Kedrov, F. Kienberger, D.J. Muller, P. Hinterdorfer, Free energy of membrane protein unfolding derived from single-molecule force measurements, Biophys. J. 93 (2007) 930–937.
[2] Y. Pan, L. Brown, L. Konermann, Mapping the structure of an integral membrane protein under semi-denaturing conditions by laser-induced oxidative labeling and mass spectrometry, J. Mol. Biol. 394 (2009) 968–981.
[3] J.P. Whitelegge, C.B. Gundersen, K.F. Faull, Electrospray-ionization mass spectrometry of intact intrinsic membrane proteins, Protein Sci. 7 (1998) 1423–1430.
[4] P.J. Booth, J. Clarke, Membrane protein folding makes the transition, Proc. Natl. Acad. Sci. U. S. A. 107 (2010) 3947–3948.
[5] U. Mayor, C.M. Johnson, V. Daggett, A.R. Fersht, Protein folding and unfolding in microseconds to nanoseconds by experiment and simulation, Proc. Natl. Acad. Sci. U. S. A. 97 (2000) 13518–13522.
[6] J.U. Bowie, Solving the membrane protein folding problem, Nature 438 (2005) 581–589.

[7] N.H. Joh, A. Min, S. Faham, J.P. Whitelegge, D. Yang, V.L. Woods, J.U. Bowie, Modest stabilization by most hydrogen-bonded side-chain interactions in membrane proteins, Nature 453 (2008) 1266–1270.
[8] K.R. Mackenzie, Folding and stability of alpha-helical integral membrane proteins, Chem. Rev. 106 (2006) 1931–1977.
[9] P.J. Booth, P. Curnow, Membrane proteins shape up: understanding in vitro folding, Curr. Opin. Struct. Biol. 16 (2006) 480–488.
[10] D.E. Otzen, P. Sehgal, L.W. Nesgaard, Alternative membrane protein conformations in alcohols, Biochemistry 46 (2007) 4348–4359.
[11] D.E. Otzen, Mapping the folding pathway of the transmembrane protein DsbB by protein engineering, Protein Eng. Des. Sel. 24 (2010) 139–149.
[12] D.E. Otzen, Folding of DsbB in mixed micelles: a kinetic analysis of the stability of a bacterial membrane protein, J. Mol. Biol. 330 (2003) 641–649.
[13] P. Sehgal, D.E. Otzen, Thermodynamics of unfolding of an integral membrane protein in mixed micelles, Protein Sci. 15 (2006) 890–899.
[14] P. Curnow, P.J. Booth, Combined kinetic and thermodynamic analysis of alpha-helical membrane protein unfolding, Proc. Natl. Acad. Sci. U. S. A. 104 (2007) 18970–18975.
[15] F.W. Lau, J.U. Bowie, A method for assessing the stability of a membrane protein, Biochemistry 36 (1997) 5884–5892.
[16] F.N. Barrera, M.L. Renart, J.A. Poveda, B. de Kruijff, J.A. Killian, J.M. Gonzalez-Ros, Protein Self-Assembly and Lipid Binding in the Folding of the Potassium Channel KcsA, Biochemistry 47 (2008) 2123–2133.
[17] K.S. Huang, H. Bayley, M.J. Liao, E. London, H.G. Khorana, Refolding of an integral membrane protein. Denaturation, renaturation, and reconstitution of intact bacteriorhodopsin and two proteolytic fragments, J. Biol. Chem. 256 (1981) 3802–3809.
[18] P.J. Booth, S.L. Flitsch, L.J. Stern, D.A. Greenhalgh, P.S. Kim, H.G. Khorana, Intermediates in the folding of the membrane protein bacteriorhodopsin, Nat. Struct. Biol. 2 (1995) 139–143.
[19] A.R. Curran, R.H. Templer, P.J. Booth, Modulation of folding and assembly of the membrane protein bacteriorhodopsin by intermolecular forces within the lipid bilayer, Biochemistry 38 (1999) 9328–9336.
[20] E.L. Compton, N.A. Farmer, M. Lorch, J.M. Mason, K.M. Moreton, P.J. Booth, Kinetics of an individual transmembrane helix during bacteriorhodopsin folding, J. Mol. Biol. 357 (2006) 325–338.
[21] D.M. Cortes, E. Perozo, Structural dynamics of the *Streptomyces lividans* K+ channel (SKC1): secondary structure characterization from FTIR spectroscopy, Biochemistry 36 (1997) 10343–10352.
[22] F.N. Barrera, M.L. Renart, M.L. Molina, J.A. Poveda, J.A. Encinar, A.M. Fernandez, J.L. Neira, J.M. Gonzalez-Ros, Unfolding and refolding in vitro of a tetrameric, alpha-helical membrane protein: the prokaryotic potassium channel KcsA, Biochemistry 44 (2005) 14344–14352.
[23] E. van den Brink-van der Laan, V. Chupin, J.A. Killian, B. de Kruijff, Stability of KcsA tetramer depends on membrane lateral pressure, Biochemistry 43 (2004) 4240–4250.
[24] E. van den Brink-van der Laan, V. Chupin, J.A. Killian, B. de Kruijff, Small alcohols destabilize the KcsA tetramer via their effect on the membrane lateral pressure, Biochemistry 43 (2004) 5937–5942.
[25] A. Malmendal, J. Underhaug, D.E. Otzen, N.C. Nielsen, Fast mapping of global protein folding states by multivariate NMR: a GPS for proteins, PLoS One 5 (2010) e10262.
[26] J.A.A. Demmers, A. van Dalen, B. de Kruijff, A.J.R. Heck, J.A. Killian, Interaction of the K+ channel KcsA with membrane phospholipids as studied by ESI mass spectrometry, FEBS Lett. 541 (2003) 28–32.
[27] M. Liu, X.- Mao, C. Ye, H. Huang, J.K. Nicholson, J.C. Lindon, Improved WATERGATE pulse sequences for solvent suppression in NMR spectroscopy, J. Magn. Reson. 132 (1998) 125–129.
[28] W.J. Dunn III, D.R. Scott, W.G. Glen, Principal components analysis and partial least squares regression, Tetrahedron Comput. Method. 2 (1989) 349–376.
[29] S. Wold, Cross-validatory estimation of the number of components in factor and principal components models, Technometrics 20 (1978) 397–405.
[30] G. Gente, C. La Mesa, Water–trifluoroethanol mixtures: some physicochemical properties, J. Solution Chem. 29 (2000) 1159–1172.
[31] J. García de la Torre, M.L. Huertas, B. Carrasco, Calculation of hydrodynamic properties of globular proteins from their atomic-level structure, Biophys. J. 78 (2000) 719–730.
[32] A. Ortega, D. Amorós, J. García de la Torre, Prediction of hydrodynamic and other solution properties of rigid proteins from atomic- and residue-level models, Biophys. J. 101 (2011) 892–898.
[33] J.Y. Kim, S.H. Ahn, S.T. Kang, B.J. Yoon, Electrophoretic mobility equation for protein with molecular shape and charge multipole effects, J. Colloid Interface Sci. 299 (2006) 486–492.
[34] J. Pedersen, A flux- and background-optimized version of the NanoSTAR small-angle X-ray scattering camera for solution scattering, J. Appl. Crystallogr. 37 (2004) 369–380.
[35] O. Glatter, A new method for the evaluation of small-angle scattering data, J. Appl. Crystallogr. 10 (1977) 415–421.
[36] J.S. Pedersen, S. Hansen, R. Bauer, The aggregation behavior of zinc-free insulin studied by small-angle neutron scattering, Eur. Biophys. J. 23 (1994) 227–229.
[37] C.L.P. Oliveira, M.A. Behrens, J.S. Pedersen, K. Erlacher, D. Otzen, J.S. Pedersen, A SAXS study of glucagon fibrillation, J. Mol. Biol. 387 (2009) 147–161.
[38] P. Baverback, C.L.P. Oliveira, V.M. Garamus, I. Varga, P.M. Claesson, J.S. Pedersen, Structural properties of beta-dodecylmaltoside and C12E6 mixed micelles, Langmuir 25 (2009) 7296–7303.
[39] P. Debye, Dispersion of Rontgen rays, Ann. Phys. Leipzig 46 (1915) 809–823.
[40] C. Spearman, "General intelligence" objectively determined and measured, Am. J. Psychol. 15 (1904) 201–292.
[41] J. Chill, J. Louis, J. Baber, A. Bax, Measurement of ^{15}N relaxation in the detergent-solubilized tetrameric KcsA potassium channel, J. Biomol. NMR 36 (2006) 123–136.
[42] M. Hirano, Y. Takeuchi, T. Aoki, T. Yanagida, T. Ide, Rearrangements in the KcsA cytoplasmic domain underlie its gating, J. Biol. Chem. 285 (2010) 3777–3783.
[43] J.H. Chill, J.M. Louis, C. Miller, A. Bax, NMR study of the tetrameric KcsA potassium channel in detergent micelles, Protein Sci. 15 (2006) 684–698.
[44] D.M. Cortes, L.G. Cuello, E. Perozo, Molecular architecture of full-length KcsA: role of cytoplasmic domains in Ion permeation and activation gating, J. Gen. Physiol. 117 (2001) 165–180.
[45] D.K. Wilkins, S.B. Grimshaw, V. Receveur, C.M. Dobson, J.A. Jones, L.J. Smith, Hydrodynamic radii of native and denatured proteins measured by pulse field gradient NMR techniques, Biochemistry 38 (1999) 16424–16431.
[46] J.R. Brender, R.P.R. Nanga, N. Popovych, R. Soong, P.M. Macdonald, A. Ramamoorthy, The amyloidogenic SEVI precursor, PAP248-286, is highly unfolded in solution despite an underlying helical tendency, Biochimica et Biophysica Acta (BBA) - Biomembranes 1808 (2011) 1161–1169.
[47] M. Buck, Trifluoroethanol and colleagues: cosolvents come of age. Recent studies with peptides and proteins, Q. Rev. Biophys. 31 (1998) 297–355.
[48] S. Kuprin, A. Graslund, A. Ehrenberg, M.H. Koch, Nonideality of water–hexafluoropropanol mixtures as studied by X-ray small angle scattering, Biochem. Biophys. Res. Commun. 217 (1995) 1151–1156.
[49] K.- Yamaguchi, H. Naiki, Y. Goto, Mechanism by which the amyloid-like fibrils of a [beta]2-microglobulin fragment are induced by fluorine-substituted alcohols, J. Mol. Biol. 363 (2006) 279–288.
[50] B. Alonso, D. Massiot, Multi-scale NMR characterisation of mesostructured materials using 1H 13C through-bond polarisation transfer, fast MAS, and 1H spin diffusion, J. Magn. Reson. 163 (2003) 347–352.
[51] F. Chiti, P. Webster, N. Taddei, A. Clark, M. Stefani, G. Ramponi, C.M. Dobson, Designing conditions for in vitro formation of amyloid protofilaments and fibrils, Proc. Natl. Acad. Sci. U. S. A. 96 (1999) 3590–3594.
[52] F. Chiti, N. Taddei, M. Bucciantini, P. White, G. Ramponi, C.M. Dobson, Mutational analysis of the propensity for amyloid formation by a globular protein, EMBO J. 19 (2000) 1441–1449.
[53] S.N. Timasheff, Protein-solvent interactions and protein conformation, Acc. Chem. Res. 3 (1970) 62–68.
[54] E.S.A.M. Al-Sherbini, M.H. Abdel-Kader, R.Y. Hamzah, Effect of binary solvents on the critical micelles concentration by using1-methyl-4-[4 '-aminostyryl]pyridinium iodide, Colloids Surf., A Physicochem. Eng. Asp. 194 (2001) 133–142.
[55] P. Sevilla Sierra, C. Civera Tejuca, F. García-Blanco, C. Díaz Oliva, J. Catalán Sierra, G. Gorostidi, Properties of 2,2,2-trifluoroethanol/water mixtures: acidity, basicity, and dipolarity, Helv. Chim. Acta 88 (2005) 312–324.
[56] M.J. Vold, Micellization process with emphasis on premicelles, Langmuir 8 (1992) 1082–1085.
[57] C. Dupuy, X. Auvray, C. Petipas, I. Rico-Lattes, A. Lattes, Anomeric effects on the structure of micelles of alkyl maltosides in water, Langmuir 13 (1997) 3965–3967.
[58] C. Cecutti, B. Focher, B. Perly, T. Zemb, Glycolipid self-assembly: micellar structure, Langmuir 7 (1991) 2580–2585.
[59] M.L. Molina, F.N. Barrera, A.M. Fernandez, J.A. Poveda, M.L. Renart, J.A. Encinar, G. Riquelme, J.M.G. Gonzalez-Rose, Clustering and coupled gating modulate the activity in KcsA, a potassium channel model, J. Biol. Chem. 281 (2006) 18837–18848.
[60] F.I. Valiyaveetil, Y.F. Zhou, R. Mackinnon, Lipids in the structure, folding, and function of the KcsA K+ channel, Biochemistry 41 (2002) 10771–10777.